UV Matrix-Assisted Laser Desorption Ionization: Principles, Instrumentation, and Applications

1. Introduction

Matrix-assisted laser desorption ionization (MALDI) is, together with electrospray ionization (ESI) (see Chapter 7 (this volume): *Electrospray Ionization: Principles and Instrumentation*), one of the most widely employed ionization techniques in biological mass spectrometry (MS). MALDI was developed in the second half of the 1980s (*1,2*), and its first published applications coincided with the first reports of ESI analyses of proteins. Owing to a low degree of analyte fragmentation, MALDI and ESI are often referred to as ''soft'' ionization techniques, and as such both paved the way for one half of the 2002 Chemistry Nobel Prize—awarded for the development of soft desorption ionization methods for mass spectrometric analyses of biological macromolecules.

The origins of MALDI lie within the laser desorption (see this chapter (this volume): *Laser Desorption: Principles and Instrumentation*) and other desorption methods (see Chapter 8 (this volume): *Secondary Ionization Mass Spectrometry and Fast Atom Bombardment: Principles and Instrumentation*; *Ion and Atom Guns*; *Massive Particle Bombardment*; *Continuous-Flow Fast Atom Bombardment*; *Pulsed Fast Atom Bombardment*; *Desorption by Cf-252 Fission Fragments* and *Desorption by Ion Beams from Accelerators*), which had as goal the development of sensitive techniques for the intact desorption/ionization of labile analytes. There are several reasons why MALDI-MS has become so popular. Among these are high analytical sensitivity, the applicability to a wide range of different compounds, easy-to-interpret mass spectra, simple sample preparation protocols, and a relatively high tolerance towards contaminants and salt contents in the sample.

The underlying idea of MALDI is the intact co-desorption of analyte molecules with a molecular excess of matrix molecules, which exert a crucial impact on the overall characteristics of the desorption/ionization process. Choosing the right analyte–matrix system is pivotal in MALDI and has been the focus of many studies for developing better MALDI analysis protocols (see this chapter: *Matrix-Assisted Laser Desorption Ionization: Matrix Design, Choice, and Application* and the following tutorials). However, most of these were ''trial and error'' studies and some of the most successful matrices (e.g., 2,5-dihydroxybenzoic acid, 2,5 DHB, and α-cyano-4-hydroxycinnamic acid, CHCA) were found empirically rather than by prediction.

The MALDI process as a whole is highly convoluted. Although desorption and ionization are often discussed separately (see Sections 4 and 5), one needs to be reminded that many aspects of both processes are coupled and occur at the same time. Moreover, the exact desorption/ionization pathways critically depend on the material properties of the compounds and on the laser irradiation parameters.

The lasers most often used for MALDI-MS are pulsed ultraviolet (UV) lasers with wavelengths close to the maximum UV absorption of the matrix (e.g., 337 nm, nitrogen gas laser; and 355 nm, frequency-tripled Nd:YAG solid state laser) and pulse durations of 1–10 ns. Other lasers and laser wavelengths can be used for MALDI-MS but less frequently owing to generally inferior MALDI and/or laser performance at these wavelengths. Hence, UV-MALDI at the above wavelengths is the predominant MALDI method in commercially available MALDI-MS instrumentation and in the main application areas of biological mass spectrometry (e.g., in proteomics: see Chapter 1 (Volume 2): *Proteomies: An Overview*).

There are, however, specific applications, in which a particular laser–matrix combination can be superior to the typically employed MALDI protocols and setups. For instance, specific UV-MALDI matrices only work at lower laser wavelengths such as the frequency-quadrupled Nd:YAG laser wavelength of 266 nm whereas infrared (IR)-MALDI with its wider range of matrices is often more successful in the intact detection of labile and large molecules (see this chapter: *Infrared Matrix-Assisted Laser Desorption Ionization*) (*3,4*).

MALDI ion sources can now be found on a variety of MS instruments including those typically used for ESI: quadrupole time-of-flight (Q-TOF) and ion trap instruments. Nonetheless, axial TOF instruments are most commonly used for many reasons (e.g., high analytical sensitivity and robustness). MALDI mass spectrometers are further discussed in Section 3.

2. Basic Aspects of Performing MALDI-MS

2.1 Sample Preparation

One of the main reasons for the popularity of MALDI-MS is its ease of analysis—its simple sample preparation, high tolerance to contaminants, and facile ion generation. The simplest and most commonly used of all sample preparations is called the ''dried droplet'' method (*5,6*). This method consists of two steps, the spotting of the analyte and matrix solution on the MALDI target and the subsequent evaporation of the volatile solvents. Given that analyte and matrix solutions are usually prepared separately, the mixing of both solutions can be either done prior to the spotting or directly on the MALDI target by applying typically 0.5–1 μL of each solution in short succession. The drying (i.e., the evaporation of the volatile solvents) in a normal lab environment is perfectly adequate although a mild stream of air is

often used to promote the drying process. Typical parameters for the ''dried droplet'' method can be found in Table 1.

The distinctive feature of MALDI, the matrix, needs to provide sufficient energy absorption at the chosen laser wavelength. Besides this pivotal role, some further important functions must be provided by a functional matrix. Among these is the sufficient ''dilution'' of analyte molecules in the matrix crystal to prevent analyte agglomeration and to facilitate molecular desorption. For peptides, for example, the useful analyte-to-matrix ratio range is roughly between 5×10^{-2} and $\sim 10^{-8}$. This means that even less than femtomole amounts of analyte can be sufficient for successful analysis. From a practical point of view, analyte and matrix molecules must be soluble in the same solvent system. After crystallization, the samples should have a sufficiently low vacuum pressure to avoid fast evaporation in the ion source. Although in most cases, matrices are used that provide a crystalline MALDI sample, other matrix systems are available, in which the analyte compounds are not embedded in a matrix crystal but desorption is rather initiated from a liquid matrix–analyte solution (see this chapter: *Ionic Liquids as Matrices for Matrix-Assisted Laser Desorption Ionization* and Refs (*7,8*)) or from a pressed pellet preparation of finely ground analyte and matrix powder (see this chapter: *Solvent-Free Matrix-Assisted Laser Desorption Ionization*). Being by far the most widely used preparation method, only crystalline analyte–matrix systems are further considered in this article.

In some applications, ''co-matrices'' and additives can improve the analytical performance (see this chapter: *Matrix-Assisted Laser Desorption Ionization: Matrix Design, Choice, and Application*). Most additives are employed either to enhance or to minimize particular types of ionization. For example, salts are frequently applied to improve the detection of synthetic polymers in their cationized form, whereas ammonium compounds are often employed to avoid cationization (e.g., of oligonucleotides) and promote analyte protonation (see this chapter: *Matrix-Assisted Laser Desorption Ionization: Matrix Design, Choice, and Application*).

2.2 Data Acquisition

MALDI-MS can be performed in either the positive- or the negative-ion mode, measuring positive or negative ions, respectively. In most MALDI-MS applications and instruments, however, the positive-ion mode usually provides higher sensitivity and spectral quality.

Once the MALDI sample is inserted into the mass spectrometer and the chosen potentials (high voltages) have been applied, the main parameter that needs to be optimized either individually by the operator or via a computer-controlled fuzzy logic is the laser intensity. In axial TOF instruments (see Section 3.1), the laser fluence (i.e., pulse energy per irradiated area) critically determines the mass-resolving power such that it is typically adjusted to values only somewhat above the ion detection ''threshold.'' For the corresponding laser energy ''threshold,'' the value is usually determined by significant analyte ion detection above the noise level (i.e., a ratio of analyte signal-to-noise of at least 2:1). The laser energy is typically adjusted to values slightly (10–30%) above this ''threshold'' value as a compromise between maximizing the analyte signal while keeping the ''chemical'' noise and matrix ion signals low (see below). This setting will allow the detection of a sufficient number of ions, generating ion signals with good signal-to-noise ratio and ideally a symmetrical monoisotopic ion profile. To improve the spectral quality further, up to a hundred or more spectra are usually accumulated. In axial TOF instruments the accumulation of spectra, however, can also result in a

Table 1
Typical irradiation parameters and sample preparation protocol for UV-MALDI

Laser wavelength:	337 nm (nitrogen laser)
	355 nm (frequency-tripled Nd:YAG laser)
Laser focus:	20–200 μm (diameter)
Laser fluence:	50–500 $J\,m^{-2}$
Laser pulse duration:	1–10 ns
Laser irradiance:	1×10^6–5×10^7 $W\,cm^{-2}$
''Dried droplet'' sample preparation protocol:	
Mix 0.5–1 μL of analyte solution with 0.5–1 μL of 10 $g\,L^{-1}$ matrix solution directly on the sample holder (target) and dry	
Matrices (for polypeptide analysis):	
2,5-Dihydroxbenzoic acid (2,5-DHB)	
α-Cyano-4-hydroxycinnamic acid (CHCA)	
Matrix/analyte solvents:	
Water, acetonitrile and various solvent mixtures	

decrease of the mass resolution and accuracy due to the changing topological properties of the sample between laser shots.

Whereas some MALDI preparation methods produce spatially rather homogeneous analyte distributions, matrices like 2,5-DHB and 3-hydroxypicolinic acid (a matrix widely used in the analysis of oligonucleotides) come along with a typical "sweet spot" effect. The "sweet spot" is a position at which a particularly high analyte ion signal is obtained while analyte ion signals may be low or even absent at other spots.

Ionization efficiencies can substantially differ between compounds and, for example, depend on the amino acid composition in the case of peptides. Analyte molecules with relatively low ionization probability may therefore be suppressed in the presence of more easily ionized species. In the case of complex mixtures in particular, sample fractionation (in concert with sample cleanup and concentration) by chromatography prior to MALDI analysis can greatly enhance the ionization efficiency (see Chapter 3 (Volume 8): *Coupling of LC and MALDI-MS*: *Techniques*, *Instrumentation*, *and Application*).

Ion suppression also affects and complicates quantification by MALDI-MS. Other factors making quantification difficult are the variations in sample morphology and composition and a possibly nonlinear response of the signal intensity to a changing analyte concentration. For these reasons, MALDI-MS is generally a much less suitable method for quantitative analysis than other analytical techniques including ESI-MS (e.g., see Chapter 1 (Volume 2): *Quantitative Proteomics via Stable Isotope Dilution* and Chapter 5 (Volume 3): *Quantitative Analysis of Biological Samples*). However, the addition of a reference analyte with similar ionization properties as the compounds under investigation or the use of liquid matrices may facilitate quantitative analysis.

2.3 Data Analysis

Although specific aspects of data analysis are described in more details in the respective MALDI application articles, it is important to discuss some of the basics here. In general, one needs to be aware of the instrumental and process-inherent effects that often concomitantly influence the final spectrum and its quality. Some of the main features that can often be seen in MALDI mass spectra are shown in Fig. 1a. It is a typical positive-ion mode axial reflector TOF mass spectrum of a peptide mixture.

One of the main characteristics of MALDI-MS is the detection of predominately singly charged intact quasimolecular ions such as protonated molecules (e.g., $[A+H]^+$ as seen in Fig. 1a,b,). Depending on the analyte and the matrix and sample purity, other singly charged quasi-molecular ions such as sodiated and potassiated molecules ($[A+Na]^+$ and $[A+K]^+$) are also frequently seen. Particularly in the analysis of glycans and synthetic polymers, metal-cationized analyte ions are preferentially formed and detected (see Fig. 1c), whereas cation adduct ions such as $[A+Na]^+$ and $[A+K]^+$ are undesirable in the analysis of peptides and proteins, whose predominant ion formation channel is based on protonation.

Although singly charged analyte ions are predominately seen in MALDI-MS, multiply charged species are sometimes observed. Particularly, larger molecules above 10 000 Da can accommodate more than just one charge without fragmenting during the analysis. This behavior is demonstrated in Fig. 1d showing the mass spectrum of human transferrin, an approximately 80 kDa protein.

Another important feature of MALDI is the generation of matrix ions. At low to intermediate laser fluences, these ions are readily observable as distinct species in the low matrix mass range (Fig. 1a). Radical matrix ions $M^{\bullet+}$, protonated matrix molecules $[M+H]^+$, and matrix ions undergoing a loss of water $[M-H_2O+H]^+$ often form the base peaks in the positive-ion mode, whereas either $M^{\bullet-}$, $[M-H]^-$, or $M-2H]^{\bullet-}$ matrix ions typically give rise to the base peaks in the negative-ion mode. The exact composition of this set of ions largely depends on the matrix used. Due to their high photochemical reactivity, many decomposition products are also formed. With increasing laser intensity, abundant matrix cluster ions are generated that eventually produce a strong and often barely resolved background (Fig. 1b). In axial TOFMS, this unspecific background can eventually stretch over the entire low-to-intermediate mass range and can render the detection of genuine analyte ion signal in the low mass range difficult.

Matrix oligomers and clusters that are initially formed upon material ejection also undergo fragmentation reactions. All types of fragments including those from matrix, analyte, and contaminant-related ions contribute to the unspecific "chemical" background or noise level. In many cases, this "chemical" noise determines the limit of detection and the analytical sensitivity. This is a particular problem in axial TOF instruments where the elimination of these sources of "chemical" noise is limited.

2.4 Fragmentation

Although MALDI is a "soft" ionization technique, there is still scope for fragmentation. This can, for instance, be initiated by high-energy collisions with plume constituents during the initial acceleration in the ion source. The considerable amount of internal energy imparted to the molecules during MALDI, however, inevitably leads to a certain degree of mainly unimolecular fragmentation. This type of fragmentation can occur at different times after the desorption event and is often called metastable decay because most of this fragmentation is not prompt.

Metastable decay significantly contributes to the "chemical" background noise.

Depending on the specific time point, metastable decay occurs at different locations within the mass spectrometer. If the decay occurs after the ions have left the source region, it is commonly called post-source decay (PSD) (see Chapter 3 (Volume 1): *TOF and RTOF*). PSD leads to unfocused (unresolved) lower molecular fragment ion signals in conventional reflector TOF mass spectrometers (e.g., see, Fig. 1b). Hence, taking the increased "chemical" noise into account, metastable decay can seriously restrict the analytical performance. As a consequence, many mass spectrometer designs incorporate elements for the elimination of metastable decay unless they are used for the acquisition of fragmentation spectra (e.g., tandem mass spectrometry—see Section 2.5).

The type of analyte, choice of matrix, and the ion extraction conditions also affect the degree of metastable decay. With respect to the matrix, one distinguishes between "hot" and "cold" indicating the higher and lower degree of ion fragmentation, respectively (see this chapter: *Matrix-Assisted Laser Desorption Ionization: Matrix Design, Choice, and Application*). Metastable decay can range from a few percent, as typical for peptides that are analyzed by using "cold" matrices, to values eventually approaching hundred percent (e.g., when using "hot" matrices in the case of sialylated glycopeptides).

In axial TOFMS, ions spend most of their flight time in the field-free drift region and, thus, predominantly undergo unimolecular fragmentation there (Fig. 2). Given that these fragment ions have the same velocity as their precursors, and the overall flight time is identical for both species, even compounds, which are very labile under MALDI conditions (e.g., oligonucleotides and sialylated glycans), can still be analyzed in linear TOF mode (green ion trajectory in Fig. 2a). Metastable fragment ions may also be separated according to their m/z value in additional electrical fields, as in a reflector (red trajectory in Fig. 2b), and be used to obtain structural information. This forms the basis of PSD analysis (see Chapter 2 (Volume 2): *Post Source Decay MALDI in Peptide Analysis*) and is further discussed in Sections 2.5 and 3.1.

Although it is common to classify fragmentation according to its occurrence either by time or location in the mass spectrometer, one needs to be reminded that various types of fragmentation can be present. While it is evident that PSD mainly consists of metastable decay, others such as prompt fragmentation and in-source decay (ISD) can lead to significantly different fragmentation spectra in axial TOF instruments. Moreover, the types of dominant fragmentation in these cases are not necessarily unimolecular.

Prompt fragmentation (at the time of the desorption event) and ISD (shortly after the desorption event; i.e., < 500 ns) (*9,10*) occur at much shorter time scales than PSD and well within the time frame of ion extraction. Therefore, the resulting fragment ions are usually well focused in all MALDI instruments, making it sometimes difficult to decide whether the associated ion signals are due to fragmentation, pre-fragmentation that occurred during sample preparation, or to genuine sample components. Obviously, all types and classes of MALDI fragmentation are important for the design of MALDI-MS and tandem MS (MS–MS) instruments.

2.5 Tandem Mass Spectrometry

For MALDI-MS–MS, both the naturally occurring decay and operator-controlled dissociation are commonly utilized. After MALDI was invented, PSD was soon exploited as the first method for obtaining structural information for peptides (e.g., see Chapter 2 (Volume 2): *Post-source Decay MALDI in Peptide Analysis*). To achieve increased fragmentation in PSD analysis, "hot" matrices and high laser intensities well above the precursor ion detection "threshold" are usually used. For peptide sequencing, PSD of singly charged MALDI ions predominately leads to complex ensembles of a-, b-, and y-type fragment ions and many internal fragment and immonium ions.

One alternative to PSD is ISD analysis, which is occasionally used in axial TOF instruments (*9,10*). The main ISD fragment ions, particularly for larger polypeptides, are c-, z-, and y-type ions. ISD product-ion spectra are remarkably similar to those obtained by electron-capture dissociation (see Chapter 2 (Volume 2): *Top-down Approach to Characterization of Proteins*) (*11*). An advantage of ISD is that larger polypeptides and even proteins can also be analyzed, whereas the practical upper mass limit for PSD analysis is about 3000 Da. ISD spectra are usually less complex than PSD spectra but the sensitivity is typically far inferior.

There are other methods that utilize PSD by applying analyte derivatization to direct the decay into specific fragmentation channels. For instance, peptide charge-derivatization using sulfonic acid functionalities at the N-terminus takes advantage of a "mobile" proton that promotes amide peptide backbone cleavage and, thus, predominately afford y-type fragments (*12*). Fragmentation is not only increased but also exceedingly specific resulting in vastly increased sensitivity and simpler fragment ion spectra that are easy to interpret (see Chapter 1 (Volume 2): *Derivatization of Peptides for Analysis*).

Lastly, commonly used and more generic dissociation techniques can also be employed in MALDI-MS–MS. In particular, low-energy (kinetic particle energy of less than 500 eV) collision-induced dissociation (CID) can be employed (e.g., see Chapter 2 (Volume 2): *Sequence Analysis: Low Energy MS–MS–Peptide*

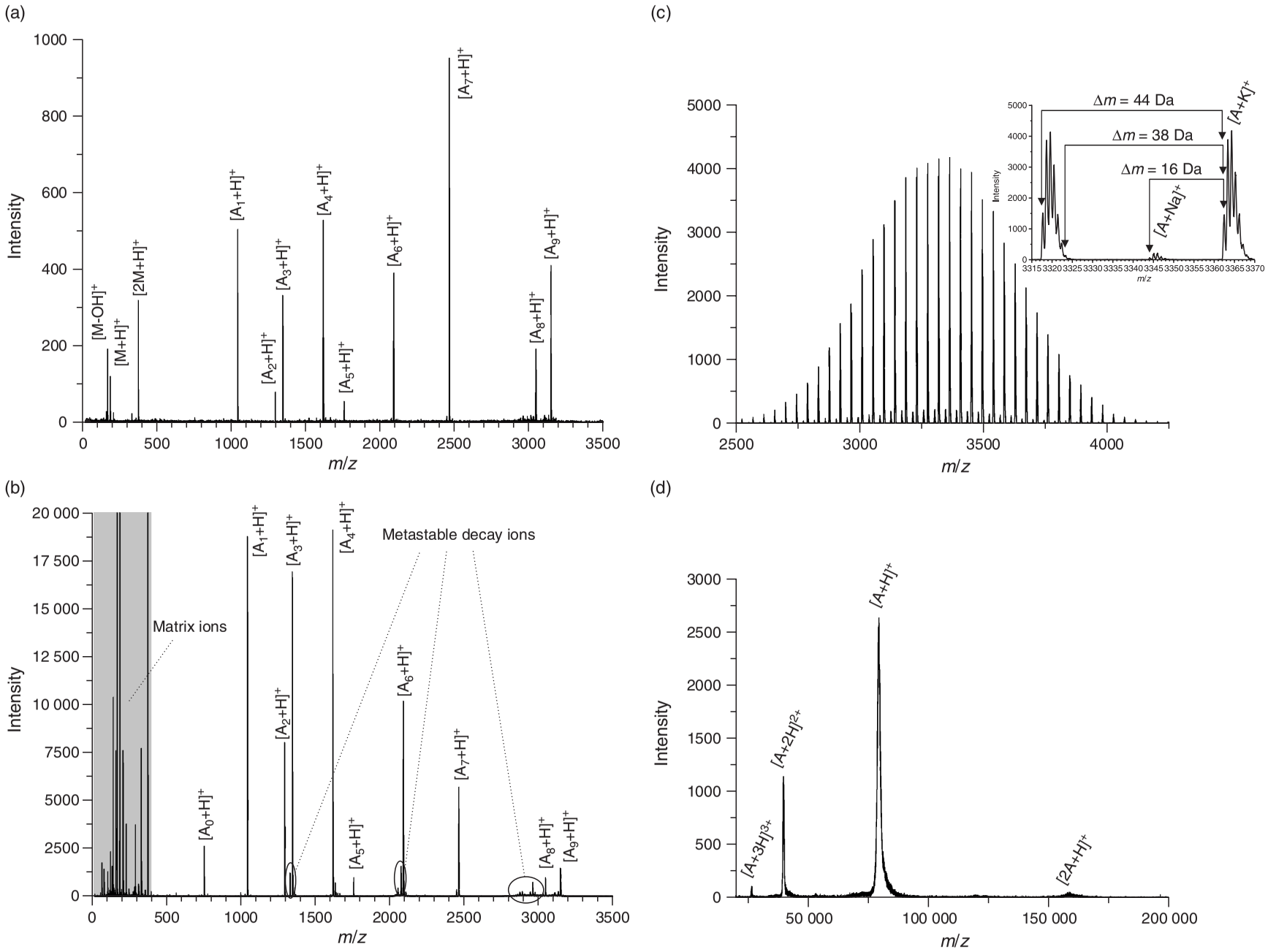
(a)
Intensity
m/z
[M-OH]+
[M+H]+
[2M+H]+
[A1+H]+
[A2+H]+
[A3+H]+
[A4+H]+
[A5+H]+
[A6+H]+
[A7+H]+
[A8+H]+
[A9+H]+
(b)
Intensity
m/z
Matrix ions
Metastable decay ions
[A0+H]+
[A1+H]+
[A2+H]+
[A3+H]+
[A4+H]+
[A5+H]+
[A6+H]+
[A7+H]+
[A8+H]+
[A9+H]+
(c)
Intensity
m/z
Δm = 44 Da
Δm = 38 Da
Δm = 16 Da
[A+K]+
[A+Na]+
(d)
Intensity
m/z
[A+3H]3+
[A+2H]2+
[A+H]+
[2A+H]+

Sequence Interpretation). In Q-TOF mass spectrometers that have both an ESI and a MALDI ion source, low-energy CID can be applied to ions formed by either ESI or MALDI (see Section 3.2). The typical difference in the charge-state of the ions formed by these two ionization techniques, however, results in significantly different product-ion spectra (*13*). Singly charged peptide ions, as are usually formed by MALDI, lead to a more complex product-ion spectrum with fewer y-type ions than in spectra of multiply charged peptide ions, which are common for ESI. MALDI axial TOF instruments offer the opportunity to perform high-energy CID owing to the high kinetic energy imparted to the ions in the ion source during their extraction (see Fig. 2c). High-energy CID facilitates charge-remote fragmentation (see Chapter 4 (Volume 4): *Charge-Remote Fragmentation: Application and Mechanism*) and can provide structural information that is not available with low-energy CID. For example, v-, w-, and d-type peptide fragment ions are virtually impossible to detect with low-energy CID whereas high-energy CID can promote these side-chain cleavages, enabling the distinction between leucine and isoleucine and other isomers (see Chapter 2 (Volume 2): *Sequence Analysis – High Energy MS–MS*).

3. MALDI Instrumentation

The pulsed nature of MALDI and its historical connection to laser desorption have made axial TOF mass spectrometers the natural choice for early MALDI-MS instruments. Later MALDI mass spectrometers utilized the great advances made in MS instrumentation as a result of the importance of biological MS in the bioanalytical sciences. Typical examples for this second generation of MALDI instruments are mass spectrometers that minimize the impact of the initial ion velocity on MS performance such as orthogonal TOF and ion-trap instruments.

3.1 Axial Time-of-Flight Mass Spectrometers

The transition from a laser desorption instrument to a MALDI instrument is seamless and requires no changes to the instrumentation (see Fig. 2). To accommodate and exploit fully the analytical power of MALDI, however, some changes are often made.

The use of a matrix usually leads to strong matrix ion signals in the low molecular mass range (see above and Fig. 1a,b). Particularly in high sensitivity measurements with a high matrix-to-analyte ratio and increased laser intensity, these signals can lead to detector saturation and low detector response for subsequent ions that strike the detector. Several methods have been devised either to remove abundant low molecular ions from the analyzer (e.g., through ion deflection—see ion deflectors in Fig. 2a) which eliminates their detection, or to lower temporarily the detector's supply voltage and, thus, its response for this mass range. Both methods result in low matrix ion signals but enhanced detector response in the analyte ion mass range. The latter method is typically applied in linear TOFMS because it also reduces the response to neutral particles potentially striking the detector.

The practical mass range for MALDI-generated ions when compared to laser desorption is far greater. This extended mass range also requires detector configurations enhanced for high mass detection. Many

Figure 1
Axial MALDI-TOF mass spectra using a nitrogen gas laser with a wavelength of 337 nm (positive-ion mode). (a) Reflector mode mass spectrum of a peptide mixture with CHCA as matrix (A_1, angiotensin II; A_2, angiotensin I; A_3, substance P; A_4, bombesin; A_5, renin substrate tetradecapeptide; A_6, ACTH clip [1–17]; A_7, ACTH clip [18–39]; A_8, ITAM γ-chain pY-peptide; A_9, somastatin 28; M, matrix). The spectrum was acquired with a laser fluence slightly above the ion detection threshold (see text for details). (b) Reflector mode mass spectrum of a peptide mixture using CHCA as matrix (A_0, bradykinin; A_1, angiotensin II; A_2, angiotensin I; A_3, substance P; A_4, bombesin; A_5, renin substrate tetradecapeptide; A_6, ACTH clip [1–17]; A_7, ACTH clip [18–39]; A_8, ITAM γ-chain pY-peptide; A_9, somastatin 28). The spectrum was acquired with a laser fluence well above the ion detection threshold (see text for details). As a consequence, matrix ion signals are elevated and saturated, matrix ion clusters are formed and (metastable) analyte decay is increased as demonstrated by the loss of water for some peptides (e.g., substance P and ACTH clip [1–17]), the significant fragmentation of the labile ITAM γ-chain pY-peptide and the relatively lower ion signals for high-mass peptides. (c) Reflector mode mass spectrum of PEG 3400 with 2,5-DHB as matrix. The addition of small amounts of KBr enhances PEG ionization and leads almost exclusively to potassium cationization. For peptides, similar amounts of KBr would, if at all, only slightly shift the ionization from protonation to potassium cationization. The inset shows two specific polymers with the mass difference Δm of 44 Da, corresponding to the mass of the ethylene glycol repeating unit. Some sodium cationization is evident by ion signals 16 Da lower than the potassiated ion signals. Protonated molecule signals, however, are insignificant as indicated by the arrows for $\Delta m = 38$ Da. (d) Linear mode mass spectrum of human transferrin with 2,5-DHB as matrix. The spectrum clearly shows the multiply charged transferrin ions ($[A + 3H]^{3+}$ and $[A + 2H]^{2+}$) with the singly charged monomer ($[A + H]^{+}$) still being most abundant whereas the singly charged dimer ($[2A + H]^{+}$) is barely observable.

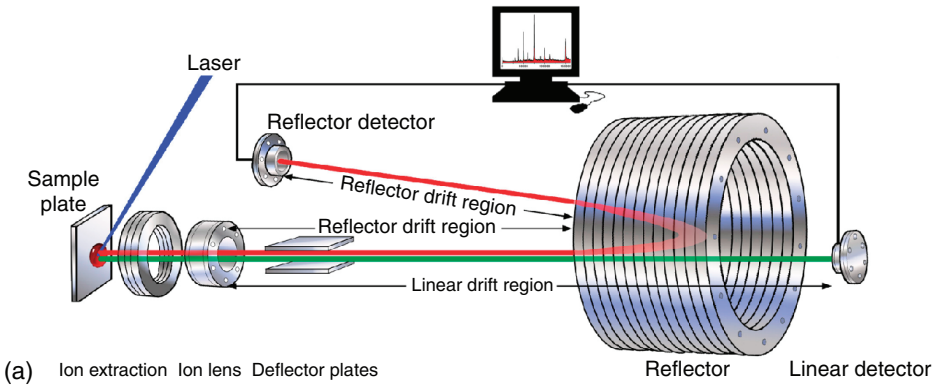
Laser
Reflector detector
Sample plate
Reflector drift region
Reflector drift region
Linear drift region
(a) Ion extraction Ion lens Deflector plates
Reflector
Linear detector

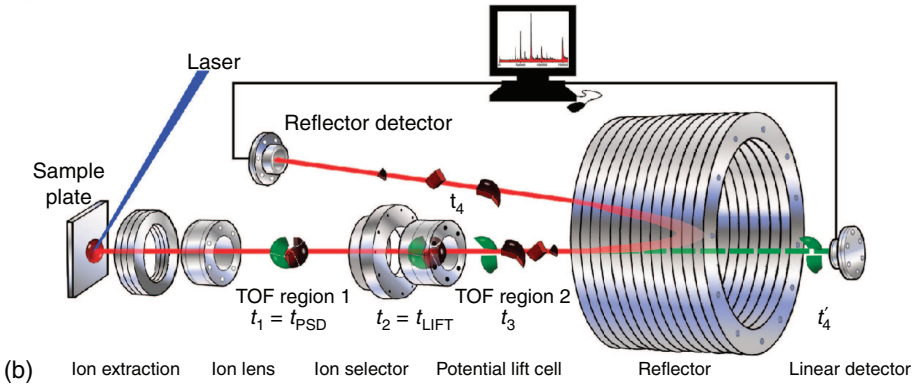
Laser
Reflector detector
Sample plate
t_4
TOF region 1
$t_1 = t_{PSD}$
$t_2 = t_{LIFT}$
TOF region 2
t_3
t'_4
(b) Ion extraction Ion lens Ion selector Potential lift cell Reflector Linear detector

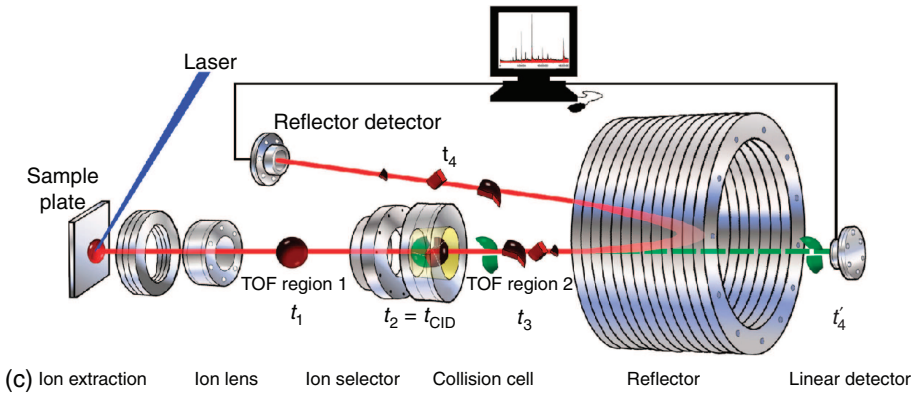
Laser
Reflector detector
Sample plate
t_4
TOF region 1
t_1
$t_2 = t_{CID}$
TOF region 2
t_3
t'_4
(c) Ion extraction Ion lens Ion selector Collision cell Reflector Linear detector

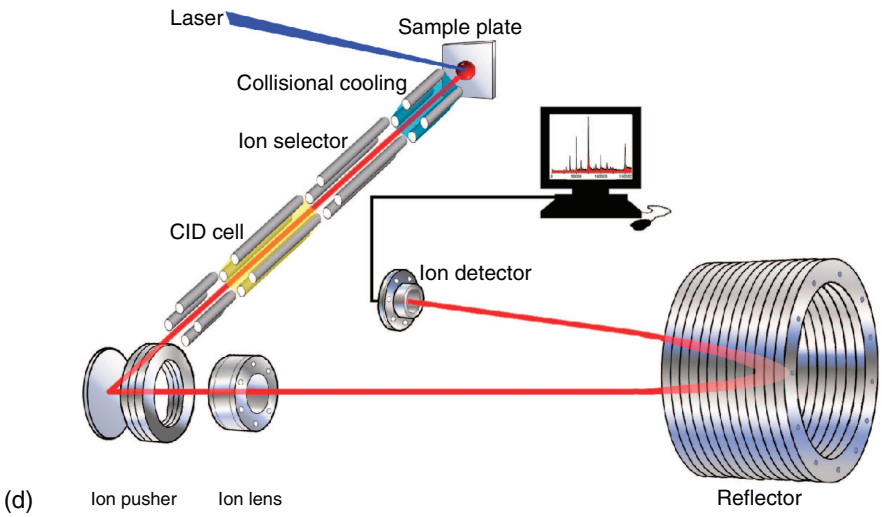
Laser
Sample plate
Collisional cooling
Ion selector
CID cell
Ion detector
(d) Ion pusher Ion lens
Reflector

detectors based on electron cascade generation only provide a low secondary ion/electron yield and, hence, a low ion signal when high-mass ions strike the detector with low velocity. To increase the secondary ion/electron yield, a "post-acceleration" dynode is often mounted separately in front of the detector. The application of a high potential to this dynode gives the ions a more energetic impact and a higher secondary ion/electron yield (i.e., higher ion signal; see also Chapter 3 (Volume 1): *TOF and RTOF*). "Post-acceleration" is essential for the analysis of large biomolecules above 50–100 kDa. However, most commercial instruments are not equipped with "post-acceleration," owing to the decreased mass resolution and accuracy, its greater technical demands, higher costs, and little benefit for the detection of low molecular ions such as peptide ions (e.g., as in proteomics).

Given that axial TOF mass spectrometers are usually operated with high extraction fields in the ion source, the entire instrument needs to be under high vacuum (typically $<10^{-6}$ hPa). High extraction field strengths and potentials provide advantages for ion detection (see above) and overall instrumental performance, particularly with respect to time-lag focusing using delayed ion extraction. The introduction of delayed ion extraction using pulsed high voltages in the mid-1990s tremendously increased both the mass resolving power ($>10\,000$) and the mass accuracy (10–50 ppm) (see Chapter 3 (Volume 1): *TOF and RTOF*).

MS–MS on axial TOF mass spectrometers is usually undertaken by using PSD or CID (Fig. 2b,c). In both cases, a precursor ion selector is employed to select ions with a given TOF acquired in the first drift region. These ions are subjected to CID in a collision chamber filled with background gas (e.g., argon) whereas for PSD, no collision gas is required. In conventional reflector mass spectrometers (e.g., those equipped with a double-stage or gridless reflector), however, PSD ions are not satisfactorily focused, let alone being reflected on the detector in the case of low mass fragment ions. Hence, the reflector voltage needs to be stepped through several focal ranges, and spectra acquired in each range need to be stitched together to obtain a sufficiently resolved PSD product-ion spectrum (see Chapter 3 (Volume 1): *TOF and RTOF* and Chapter 2 (Volume 2): *Postsource Decay MALDI in Peptide Analysis*). To avoid this laborious and sample- consuming acquisition, alternative reflector TOF designs can be employed. In quadratic and curved field reflectors, most PSD fragment ions are focused, and no spectra need to be stitched together (see Chapter 3 (Volume 1): *TOF and RTOF*). The angle of acceptance for these reflectors, however, is far lower than for conventional reflectors, making them less sensitive. Moreover, PSD fragment ions are also focused and seen in the normal mass spectrum, which is undesirable for analyses of complex analyte mixtures. An alternative to higher order reflector designs is based on increasing the kinetic energy of the PSD fragment ions in a potential lift cell before they enter the reflector (see Fig. 2b) (*14*). If, after the potential lift, all PSD fragment ions possess at least 60–70% of the kinetic energy of their precursor ion, even conventional reflectors are able to adequately reflect and focus them on the detector. A major disadvantage of the PSD method is that mass accuracy is relatively low ($\sim$0.2 Da) even under optimal conditions.

3.2 Orthogonal Time-of-Flight Mass Spectrometers

With the rise of proteomics, new developments in MS instrumentation and their integration in complex bioanalytical workflows became necessary. As a consequence, new types of MALDI mass spectrometers with a general emphasis on the hybridization and hyphenation of technologies were developed. In 2000,

Figure 2
Schemes of MALDI-TOF mass spectrometers. (a) Axial MALDI reflector TOF mass spectrometer. After ion extraction ions are further guided and focused before entering the field-free drift region. Matrix ion signals can be minimized by using ion deflection plates and/or by temporarily lowering the detector voltage to avoid detector saturation. In the reflector mode, energy-focusing increases the mass resolving power, which can be further enhanced by time-lag focusing using delayed ion extraction (see Chapter 3 (Volume 1): *TOF and RTOF*). (b) Axial MALDI-PSD TOF-TOF tandem mass spectrometer. Ions may fragment through metastable decay in the first drift region (t_1). After ion selection, the kinetic energy of the fragment ions (and unfragmented precursor ions) will be increased through a potential lift (t_2) sufficiently strong for all ions to be reflected and focused on the reflector detector (see text for details). Alternatively, a set of spectra recorded at stepwise-lowered reflector voltages can be stitched together. In this case and for higher order reflector designs that are capable of focusing all PSD fragment ions, no potential lift cell is required. (c) Axial MALDI-CID TOF-TOF tandem mass spectrometer. From the ion selector, transmitted precursor ions are fragmented by collisional activation in the collision cell (t_2). The fragment ions are then conventionally separated and analyzed by the subsequent reflector TOF mass analyzer. (d) Orthogonal MALDI-(CID) Q-TOF (tandem) mass spectrometer. After MALDI ions are formed, collisional cooling thermalizes their initial ion velocity. Ions are orthogonally injected into the TOF ion pusher region and conventionally analyzed by TOFMS at high repetition frequencies. Precursor ion selection and fragmentation in a CID cell facilitate MS–MS measurements.

several publications reported the coupling of MALDI ion sources to orthogonal TOF and hybrid Q-TOF instruments (Fig. 2d) (*15–17*). These instruments employ effective collisional cooling and ion manipulation to dampen the ion motions in all directions, reducing the initial ion velocity distribution and internal ion energy acquired from the MALDI process and, consequently, enhancing ion survival rates and improving the ion beam quality and overall MS performance (*18*). When the ions enter the TOF mass analyzer after orthogonal injection (see Fig. 2d), the initial velocity distribution is marginal and MS performance is largely dependent on the analyzer function and less on the ionization process or ion source conditions. Mass spectral parameters such as mass resolving power, mass measurement accuracy and precision are virtually the same whether MALDI or ESI ions are analyzed.

The relatively high ion source pressure of typically more than 10^{-2} hPa used for collisional cooling also facilitates the use of the same mass spectrometer for both ESI and MALDI with an easy swapping of ion sources. Even the use of atmospheric pressure (AP)-MALDI ion sources is possible (*15*) (see this chapter: *Atmospheric Pressure Matrix Assisted Laser Desorption Ionization (AP-MALDI)*).

Other advantages of effective collisional cooling and decoupling of the ion source from the TOF analyzer include: (i) the generation of a quasicontinuous ion beam enabling ESI beam-like measurements with high repetition TOF analysis and low peak saturation; (ii) low metastable decay, particularly at the time of the TOF measurement, producing only few additional ion signals and low signal background due to ''chemical'' noise; and (iii) a low influence of MALDI conditions on the TOF measurement, offering a greater choice of sample preparations and desorption parameter values.

Nonetheless, sensitivity is limited by the duty cycle of the pulsed TOF measurements from the quasicontinuous ion beam and, thus, theoretically lower than in axial TOF instruments, although improvements can be achieved by ion trapping and ion injection coordinated with the TOF pulsing (*19*). In addition, the low ion acceleration voltages in most orthogonal TOF instruments discriminate the detection of the larger singly charged MALDI ions. Another potential disadvantage of collisional cooling is the formation of adduct complexes between analyte ions and matrix molecules. The extent of such reactions can be considerably higher than in high-vacuum MALDI ion sources as employed in axial TOF mass spectrometers.

One important practical point that also needs to be considered for the employment of MALDI sources on instruments that were originally designed for ESI-MS and in which quadrupoles (or multipoles) are used, is the predominantly single charge state of MALDI-generated ions. In contrast to the generally multiply charged ESI ions that can mostly be analyzed (or transmitted) by quadrupoles (or multipoles) with small m/z ranges (typically m/z 0–4000) MALDI ions require quadrupoles with extended m/z ranges. Given that there are practical limits to the m/z range of a quadrupole in both sensitivity and duty cycle, most large-range quadrupoles are limited to an m/z range of up to 16 000 being also the overall upper limit for the instrument and, thus, by far lower than that of axial TOF mass analyzers. This is of particular importance for MS–MS instruments, in which usually quadrupoles (or multipoles) are employed for precursor ion selection.

Nonetheless, one of the advantages of hybrid orthogonal TOF instruments (e.g., Q-TOF) is their superior performance in MS–MS. The TOF performance is virtually unchanged between MS and MS–MS measurements, providing high mass resolving power and accuracy even in the MS–MS mode. As with ESI, CID-MS–MS measurements of MALDI-generated precursor ions can be successfully performed at high sensitivity (low femtomole amounts of sample) with efficient precursor ion selection (unit mass resolution) and low ''chemical'' noise background.

3.3 Ion Trap Mass Spectrometers

MALDI in combination with Paul ion trap mass spectrometers, also called quadrupole ion trap mass spectrometers, was reported in the early 1990s (*20–22*) (for details on Paul ion traps, see Chapter 3 (Volume 1): *Ion Traps*). As with two-dimensional quadrupoles, the wide initial velocity distribution of MALDI ions reduces the analytical performance (i.e., the trapping efficiency). Therefore, efficient dampening of the ion motions is also vital for MALDI with Paul ion traps. Abundant matrix ions pose another problem and need to be excluded from the trapping because ion traps have a limit for the maximum number of ions they can hold before space-charge effects become significant. In addition, metastable decay can be detrimental to the MS analysis considering the relatively long analysis time in ion traps.

Nonetheless, ion traps are compatible with MALDI if the above challenges are satisfactorily met. To achieve this goal, an external ion source with adequate ion transfer lines and collisional cooling is typically employed whereas the pulsed nature of ion trapping can be synchronized with the pulsed formation of MALDI ions and their transfer to the ion trap.

Similarly to quadrupole and Q-TOF mass analyzers, however, ion traps have limitations for the analysis of high m/z ions. Today's upper limit for Paul ion traps is approximately m/z 4000–6000. In principle, MALDI ions above an m/z value of 10 000 can also be detected on Paul ion traps, but only at reduced performance.

Another ion trap mass spectrometer is the Fourier transform ion cyclotron resonance (FTICR) instrument (see Chapter 3 (Volume 1): *Fourier Transform Ion Cyclotron Resonance*). Successful coupling of MALDI to FTICR instruments was first achieved in the early 1990s. In general, for MALDI-FTICR-MS one has to consider the same issues as for MALDI-MS employing Paul ion traps. The required ultrahigh vacuum (around 10^{-10} hPa) and even longer analysis times than in Paul ion traps pose additional demands on the coupling. Owing to the high kinetic energy of MALDI ions and their metastable ion decay, FTICR-MS performance was initially poor. With adequate collisional cooling, external ion accumulation and/or ion deceleration, analyte ions can be sufficiently cooled and trapped while matrix ion interference is minimized. At modest m/z value, these advances enable those advantages of FTICR as seen with ESI (i.e., extremely high mass resolving power and mass measurement accuracy at high sensitivity). The analytical performance, however, significantly degrades with increasing m/z values, making ESI with its higher charge state ions the preferred ionization technique for most applications. On the other hand, MALDI sources on FTICR mass spectrometers offer the advantage of coordinating the formation of MALDI ions with the FTICR analysis, avoiding timing problems and superfluous sample consumption as it can be the case for ESI. Specifically, offline liquid chromatography (LC)–MALDI coupled to FTICR ensures the detection of all LC-eluted components while online LC–ESI is prone to missing components that elute while the FTICR instrument is busy analyzing earlier eluents—a typical dead time effect. These issues become increasingly important in proteomic analyses, in which high proteome coverage is often required (see Volume 2).

4. The Desorption Process in UV-MALDI

MALDI is a complex process that involves optical and mechanical phenomena as well as thermodynamic and physicochemical processes of phase transition and ionization (*23,24*). Figure 3 depicts the MALDI process schematically. For conventional MALDI employing crystalline matrices and typical laser conditions, the desorption process is essentially thermally controlled. However, as outlined below, the process takes place in thermal nonequilibrium.

4.1 Importance of Irradiation and Material Parameters

To achieve optimal results, several material and irradiation parameters (see Table 1) need to be adjusted carefully. The laser-pulse duration, for example, must be sufficiently short to avoid thermal degradation of the analyte compounds. In other words, time

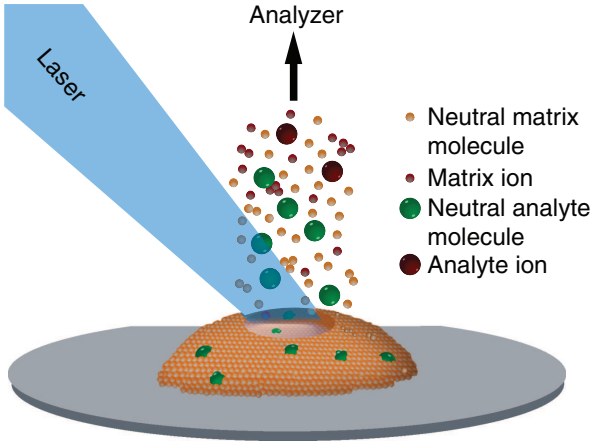

Figure 3
Scheme of the MALDI process.

constants for the desorption channel need to be small compared to those which induce thermal fragmentation. Typically, laser pulses in the low nanosecond range are employed for UV-MALDI. Lasers with even shorter pulses may be used, but generally do not lead to improved results.

The second most important irradiation parameter, the laser emission wavelength, must correspond to a high optical absorption of the matrix to achieve a high energy density in the sample. Suitable matrices exhibit molar absorptivities between 2000 and 20 000 L mol^{-1} cm^{-1} at the UV excitation wavelengths, as measured in solution. Assuming similar absolute values for matrix crystals, the laser light will be essentially absorbed within the upper 20–200 nm of the crystals. Typical matrices with conjugated aromatic systems exhibit relatively broad absorption bands of several tens of nm in width, easing the demands on the exact choice of the laser. As noted above and in the following article: *Matrix Design, Choice, and Application*, matrices with absorption bands peaking in between ~300 and 350 nm are almost exclusively employed for UV-MALDI, matching well the emission wavelengths of both the nitrogen (337 nm) and/or the frequency-tripled Nd:YAG laser (355 nm). Essentially all of the common matrices like 2,5-DHB and cinnamic acid derivatives (e.g., CHCA and sinapinic acid) belong to this group. A noteworthy drawback of the frequency-tripled Nd:YAG laser is a reduced optical absorption for a few important matrices like 3-hydroxypicolinic acid.

Low "sublimation" temperatures at which significant desorption sets in are often regarded as an advantageous parameter that helps to reduce unwanted thermal analyte degradation. This is one reason why no suitable matrix compound with extended conjugate electronic system has been found so far. The more extended systems shift the optical absorption

into the red (i.e., the visible region) but also increase the intermolecular binding strength of the molecules. Even a high temporary lattice temperature of the matrix crystal will not automatically lead to a strong internal excitation of analyte molecules. The frequency mismatch between lattice and intramolecular analyte vibrations forms a bottleneck (*25*) that effectively delays a full equilibration. Evaporative and collisional cooling within the expanding MALD(I) plume further stabilize labile analyte molecules.

With a few exceptions such as molecules carrying chromophores (e.g., cytochrome *c*), UV absorption above 300 nm is negligible for biomolecules and direct photodissociation of analyte molecules is avoided. For the following discussion, it can be assumed that, due to the low molar analyte-to-matrix ratio, most physicochemical properties of the analyte-matrix crystals are essentially identical to those of neat matrix preparations.

4.2 Energy Absorption and Relaxation

Population of the first excited singlet state (S_1) by resonant optical absorption serves as the primary excitation step. Due to the Frank–Condon principle, some excess photon energy is at this stage already converted into heat by internal conversion to vibrationally lower lying S_1 states. Fluorescence, intersystem crossing, ionization after absorption of a second photon, and photochemical reactions lead to some energy "loss," but most of the energy stored in the S_1 state is transformed radiationless by internal conversion into intramolecular lattice vibrations (i.e., heat). S_1 decay constants can be estimated from fluorescence studies to be on the order of a few 10^{-10} s (*26*). This is somewhat shorter than typical laser pulses.

Thermal relaxation times in the condensed phase τ_{th} can be estimated by

$$\tau_{th} = \frac{\rho c_p}{a\lambda_{th}}\delta^2$$

where ρ is the density of the material, c_p the specific heat, λ_{th} the thermal conductivity, and δ is the laser penetration depth. The factor a accounts for the size/geometry of the irradiated crystals and is usually between 1 and 4. Using typical material parameters, values for τ_{th} on the order of $\sim$10 ns are calculated. This is close to, but still slightly above, the laser-pulse duration. Once all energy is absorbed, the excited volume will exhibit a relatively homogeneous temperature profile with sample depth while heat dissipation out of the excited volume is low.

The laser heating is accompanied by rapid expansion of the material and, hence, by the generation of photomechanical stress. Time frames for acoustic energy relaxation are determined to the first order by the propagation time of a stress wave through the excited medium (i.e., by the ratio of the excitation depth δ and the speed of sound v_s: $\tau_{ac} = \delta/v_s$). Values for τ_{ac} are on the order of a few tens of picoseconds for typical UV-MALDI conditions, and the stress amplitudes are, therefore, too low to have any major effect. Photoacoustic stress can, however, play an important role in IR-MALDI where considerably larger laser penetration depths are found (see this chapter: *Infrared Matrix-Assisted Laser Desorption Ionization*).

Laser fluences at the ion detection threshold are on the order of a few tens to a few hundreds of joules per square meter ($J\,m^{-2}$), depending on matrix absorption and laser spot size (*27*). For typical laser spot sizes of 100–200 μm in diameter, this translates to rather equal energy densities per volume for different matrices of approximately $1 \times 10^9\,J\,m^{-3}$ at the surface of the sample. These values are close to the sublimation enthalpies. Energetically, vaporization of the surface volumes is therefore possible. Under equilibrium conditions, an energy per volume of $1 \times 10^9\,J\,m^{-3}$ corresponds to a temperature increase of some hundred Kelvin. The nonequilibrium character of the process can lead to even higher lattice temperatures. Post-ionization studies show that at fluences below the ion detection threshold, a high number of neutral molecules are already ejected (*27*).

In the rarely used suspension matrices, where the matrix usually consists of a suspending compound such as glycerol with suspended nanoparticles like cobalt or TiN, laser light absorption is decisively different (*2*) (see this chapter: *Matrix-Assisted Laser Desorption Ionization: Matrix Design, Choice, and Application*). Whereas the optical and thermodynamic properties of micrometer-sized particles do not differ much from those of the corresponding bulk material, nanoparticles with diameters below $\sim$100 nm can show different features due to surface effects like the excitation of surface plasmons. As a consequence, the optical absorption can become very high, even if the bulk material only absorbs moderately. By using nanoparticle suspension matrices, temperatures on the order of 10 000 K are reached with high heating rates (*28*).

4.3 Material Ejection

At low laser fluences below or close to the ion detection threshold, layer-by-layer sublimation from the surface forms the dominant desorption mechanism (*23*). Desorption sets in during the laser pulse and, because of the evaporative cooling, rapidly terminates after the laser pulse has ceased. Molecular desorption dominates this fluence regime, although a "selvedge region" consisting of molecules and small clusters is formed (*29*). Hence, a certain percentage of clusters will also persist in the expanding plume.

The molecular desorption rate can be approximated by an Arrhenius-like relation. Taking into account that, for nanosecond pulsed lasers, the overall

amount of ejected material can be set proportional to the desorption rate at the peak temperature, the overall desorption yield of monomeric molecules can be described by a "quasithermal" equation of the form

$$Y \sim P(A)\exp\left(\frac{-E_a}{k_B(T_0 + BF)}\right)$$

where Y is the ion yield, E_a the activation energy for the process, T_0 the initial sample temperature, and k_B the Boltzmann constant (*27*). F denotes the laser fluence, and B a conversion factor accounting for the transformation of laser pulse energy into (lattice) temperature of the sample. $P(A)$ is a pre-exponential factor that includes a (less strong) additional temperature dependence. For MALDI, there is a strong dependence of the ion yield on the laser spot size (*27*), which is also included in the prefactor.

At higher laser fluences, where the desorption rate is not sufficient to balance the energy deposition, sizable overheating occurs, and the heated material can ablate instantaneously by phase explosion (*30*). In this case, molecular desorption is accompanied by the ejection of a larger number of clusters (*29*). This mechanism can play a particularly significant role in high-pressure MALDI ion sources (see this chapter: *Atmospheric Pressure Matrix Assisted Laser Desorption Ionization (AP-MALDI)*) for which high laser fluences are frequently used. In axial TOF instruments, in which a background pressure of approximately 10^{-7} hPa is normally maintained, the useful MALDI fluence range is limited and typically reaches from the ion detection threshold to values of a factor of 2–3 above. Further increase of the laser fluence results in significant analyte fragmentation and degradation of the quality of the mass spectra. This effect is also believed to account in part for the strong spot size effect and over-proportional increase of the threshold fluence with decreasing spot size.

Whereas in conventional MALDI analyses, laser focus diameters between 50 and 200 μm are typically used, smaller diameters are important for imaging MALDI-MS applications, in which a high lateral resolution is sought (see this chapter: *Surface Analysis of Biomaterials* and Chapter 4 (Volume 2): *Profiling and Imaging Peptides and Proteins from Mammalian Tissue Sections by MALDI and Single-Cell Peptide Analysis with MALDI-MS*). Although spot sizes with a few micrometers in diameter are technically easy to realize, they lead to conditions that are apparently too destructive for the analysis. Spot sizes approaching a few micrometers in diameter, the accompanied strong increase in threshold fluence also leads to the ablation of a volume of material of several hundreds of nm in depth, thus changing the overall processes considerably. MALDI imaging is therefore mostly performed with minimal laser spot sizes of about 20 μm in diameter.

4.4 MALDI Plume Expansion

In a typical setup with a focal laser spot size of 100 μm in diameter, a layer of material of about a few to a few tens of nanometers in depth (i.e., a few to a few tens of monolayers) is desorbed per laser pulse at the ion detection threshold. The ejected molecules undergo a large number of intermolecular collisions during the phase disintegration and the plume expansion. These collisions have a significant effect on the expansion characteristics and lead to a forward-shaped MALDI plume. Average axial velocities (i.e., in the direction of ion extraction) of neutral matrix molecules are on the order of 500 m s^{-1} with a width of the velocity distribution being of a similar size (*23*). Mean velocities of MALDI ions are even higher and approach 1000 m s^{-1} (*31,32*). Thus, the ions are essentially found in the front part of the expanding MALDI plume. Radial velocity components reflect thermal values more closely and, thus, are lower than the axial ones and more mass dependent (*32*). Multiple collisions with matrix molecules accelerate the entrained analyte molecules to similar axial velocities (*31*). For large analyte molecules, this results in high kinetic energies on the order of several eletronvolts, again with similar widths of the energy distribution. This leads to a sizable reduction of the performance of axial TOF instruments and problems in ion transmission and ion trapping in quadrupole and ion trap mass spectrometers, respectively.

For high-pressure ion sources (see Sections 3.2 and 3.3), which are typically operated at a pressure of about 1 hPa and up to 1000 hPa for atmospheric pressure (AP)-MALDI (see this chapter: *Atmospheric Pressure Matrix Assisted Laser Desorption Ionization (AP-MALDI)*), collisions with the background gas lead to a rapid thermalization and a very different plume expansion character. The accompanied collisional cooling leads to a stabilization of co-desorbed analyte molecules and allows the effective use of Q-TOF and ion trap instruments for MALDI-MS (see Sections 3.2 and 3.3) even at very high laser fluences.

5. The Ionization Process in UV-MALDI

One feature that makes MALDI so attractive is that the method works well for an extraordinarily wide range of chemical compounds possessing rather dissimilar physicochemical properties. For example, MALDI can be applied to virtually all classes of biomolecules (see Volumes 2 and 3), but also to synthetic polymers (see Chapter 11 (this volume): *Synthetic Polymers*), and to many inorganics. The exact ionization pathway depends on the physicochemical properties of analyte and matrix, in particular proton affinities (PAs), gas-phase acidities (GPAs), and gas-phase basicities (GPBs). Given that these vary with the type of analyte, the choice of the matrix should be

properly adjusted to the type of compounds under investigation (see this chapter: *Matrix-Assisted Laser Desorption Ionization: Matrix Design, Choice, and Application*). The convoluted processes of desorption and ionization, involving the rapid phase transition, temporary high temperatures, and manifold energetic collisions, render it difficult to establish a simple picture of the MALDI ionization. In many cases, the matrix plays a vital role in the ionization process (e.g., as proton donor or acceptor). Owing to the high number of intermolecular collisions during the plume expansion, energetically controlled thermochemistry will in general determine the mass spectrum. Reactions thermochemically not feasible under equilibrium conditions may contribute to the overall outcome. As a consequence, surprisingly similar mass spectra (in the analyte mass region) are produced by UV- and IR-MALDI despite the very different primary ionization mechanisms in the two wavelength ranges (see this chapter: *Infrared Matrix-Assisted Laser Desorption Ionization*). Only at very low laser fluences, at which only few ions are produced, the process will be kinetically rather than energetically controlled. The transition from one regime to the other is in some cases reflected in a changing composition of matrix ion species (e.g., the ratio between radical ions and protonated molecules) in the mass spectrum.

The ion detection laser fluence threshold, at which a sufficient number of ions is generated to produce a mass spectrum, is higher by a factor of 2–3 than that for the detection of neutral molecules (*27*). Further, the dependence of the gas-phase yield on the laser fluence is stronger for ions than for neutral molecules, indicating an additional ionization process. Provided there is sufficient analyte-to-matrix ratio and detection sensitivity, analyte and matrix ions exhibit the same fluence thresholds and the same yield dependence on laser fluence (*27*). Estimations for matrix ion yields (i.e., the ratio of generated matrix ions to overall desorbed matrix molecules) range between $1{:}10^3$ and $1{:}10^5$. In cases of favorable secondary ionization conditions, the analyte ion yield is likely to be on the high side of this range or even somewhat above.

Analytes with molecular weights exceeding 10 kDa are typically observed with sizeable yields of multiply charged ions (protonated/deprotonated molecules) (see Fig. 1d). As molecules become larger in size, the charges are sufficiently separated so that the Coulomb energy of the system becomes low, and the charge sites more independent. The maximum possible charge state scales with the size of the analyte. Very large molecules such as monoclonal antibodies of molecular weight $\sim$150 kDa may carry as much as five charges with sizable intensity. The high number of collisions in the expanding MALDI plume also helps to overcome the Coulomb barrier in the primary charge separation process.

Although not fully separable, it is nevertheless helpful to differentiate between primary excitation/ionization of matrix molecules and reactions between these species, on the one side, and secondary ionization reactions between them and the analytes, on the other. One should keep in mind that in addition to these reaction schemes, involving essentially monomeric molecular species, a high percentage of molecules, at least temporarily, form dimers, oligomers, or even small clusters. Moreover, the initial matrix-analyte solid state provides an environment rather different from the final gas-phase state. This can significantly change the energetics (*33,34*).

5.1 Primary Ionization Reactions

Some possible primary ionization pathways are depicted in Table 2a. Typical ionization energies (IEs) (see Chapter 1 (this volume): *Ionization Energies*) of monomeric matrix molecules are approximately 8 eV. Numerically, two photons of either 3.68 or 3.49 eV at 337 and 355 nm, respectively, are not sufficient to cause ionization. Even though IEs can be lower by a few tens of electronvolt in the condensed phase owing to solvation effects, other processes must be involved to balance the energy requirements. For example, the thermal energy content can assist the ionization. The second excited singlet state (S_2), from which ionization can most easily be initiated, can be populated by subsequent resonant two-photon absorption. This process (reaction 2.1 in Table 2) however, probably does not apply at typical MALDI fluences of about $100\,J\,m^{-2}$ (see Table 1).

Energy pooling between neighboring excited molecules or between two excitons (mobile electron–hole pairs in the solid; reaction 2.2) forms the most likely ionization pathway. In a process called singlet–singlet (S_1–S_1) annihilation (*26*), one molecule is excited into the second excited S_2 state while the S_1 state of the second molecule is relaxed. Energy pooling may also take place as a multicenter process involving more than two molecules; this also loosens the requirements on the energetics.

Whereas the lifetimes of the first excited singlet states in the solid are only approximately 10^{-10} s for typical matrix compounds, they can extend to a few nanoseconds or more for monomeric molecules. Therefore, ionization that is delayed with respect to the laser pulse can occur during the plume expansion phase. Intersystem crossing from a singlet to a long-lived triplet state may also extend the time window for ionization.

Excited state proton transfer (ESPT; reactions 2.3) and even ground state proton transfer reactions (disproportionation reactions; reactions 2.4) from neutral matrix molecules are also theoretically possible primary MALDI ionization mechanisms (*35*). Organic molecules such as aromatic amines and phenols frequently exhibit an increased acidity upon electronic excitation; the increased acidity could allow ESPT to analyte. A sufficient yield of ground state

Table 2
Possible primary (a) and secondary (b) ion formation mechanisms in MALDI

Mechanism	Reaction		Comment
(a) *Primary ionization mechanisms*			
Single molecule multiphoton ionization	$M + n^{\bullet} h\nu \rightarrow M^{\bullet +} + e^-$	(2.1)	Feasible but with low rates at typical laser fluence values
Energy pooling (S_1–S_1-annihilation)	$M + h\nu \rightarrow M^*$ $M^* + M^* \rightarrow M^{**} + M$ $M^{**} \rightarrow M^{\bullet +} + e^-$	(2.2)	Probably the major pathway for primary matrix ionization
Excited-state proton transfer	$M + h\nu \rightarrow M^*$		Feasible for matrices with a high acidity in the exicited state, but unlikely to be a general major MALDI pathway
	$M^* + M \rightarrow [M + H]^+ + [M - H]^-$	(2.3a)	
	$M^* + A \rightarrow [A + H]^+ + [M - H]^-$	(2.3b)	
Ground-state proton transfer	$M + M \rightarrow [M + H]^+ + [M - H]^-$	(2.4a)	Sufficient proton transfer rates would require unlikely high plume temperatures. Proton transfer from matrix oligomers would energetically be somewhat less costly (*33*)
	$M + A \rightarrow [A + H]^+ + [M - H]^-$	(2.4b)	
	$M + A \rightarrow [A - H]^- + [M - H]^+$	(2.4c)	
Thermal ionization	$M + M \rightarrow M^{\bullet +} + M^{\bullet -}$	(2.5a)	A relevant pathway for nanoparticle suspension matrices but not for common MALDI
	$M \rightarrow M^{\bullet +} + e^-$	(2.5b)	
(b) *Secondary ionization mechanisms*			
Proton transfer	$[M + H]^+ + A \rightarrow M + [A + H]^+$	(2.6a)	The dominant ionization pathway for major classes of compounds (e.g., peptides and proteins). Proton transfer may proceed from a matrix ion in a ground or excited state
	$[M - H]^- + A \rightarrow M + [A - H]^-$	(2.6b)	
	$M^{\bullet +} + A \rightarrow [M - H]^{\bullet} + [A + H]^+$	(2.6c)	
Cationization other than protonation	$A + Cat^+ \rightarrow [A + Cat]^+$	(2.7a)	Relevant where proton transfer is not feasible
	$A + [M + Cat]^+ \rightarrow [A + Cat]^+ + M$	(2.7b)	
Electron transfer	$M^{\bullet +} + A \rightarrow M + A^{\bullet +}$	(2.8)	Except for special cases, not a relevant pathway

M, matrix molecule; M^*, M^{**}, singly and doubly excited matrix molecules; A, analyte molecule; Cat^+ metal cation.
Note: Reactions indicated for matrix monomers may similarly also be initiated from a matrix dimer or oligomer.

proton transfer reactions between two initially neutral matrix molecules, however, would require temperatures of a few thousand Kelvin. These transfers would be at best a small fraction provided by the high-side tail of the Boltzmann distributions. A second major argument against the general involvement of ESPT, is that some good matrices are clearly ESPT-inactive in solution and that many molecules with a high ESPT-activity fail completely as MALDI matrix. Proton transfer between a neutral matrix and an analyte molecule may also take place in a direct reaction (2.4b and c), but the requirements on the energetics are high, as discussed above. Although the latter mechanisms cannot be completely excluded to contribute to the overall ion yield, they are therefore not very likely. Furthermore, many experimental observations support energy pooling reactions as the major primary ionization mechanisms. This reaction (2.2) also explains the often detected radical ions of the matrix molecules.

In a different scenario, ions that were preformed already in the condensed phase are simply released upon desorption. With the exception of ionic compounds or metal-complexed analytes, however, the solvent state is generally not reflected in the MALDI mass spectra. Preformed negative ions are also rarely observed. Hence, for the majority of analyte compounds the ejection of preformed ions is either of little relevance, or initially desorbed ions are rapidly masked by secondary reactions taking place in the plume.

Thermal ionization (reaction 2.5) plays a decisive role in laser desorption/ionization with nanoparticle suspension matrices, where the temperature can reach peak values of 10 000 K or more. Ionization is typically assisted by the suspending matrix compound such as glycerol.

5.2 Secondary Ionization Reactions

Some possible secondary ion reactions are depicted in Table 2b. Energetically, proton transfer from either a radical matrix molecule, a protonated matrix molecule, or eventually a protonated matrix-oligomer to a neutral analyte molecule (reactions 2.6) are in many cases highly favored (e.g., in the MALDI analysis of peptides and proteins; see Fig. 1a,b,d) (*24,36*). In the negative-ion mode, the differences of the GPBs of deprotonated analytes and those of matrix anions determine whether proton detachment from a neutral analyte molecule is energetically feasible. Generally, these differences are smaller for a particular analyte species and the matrix than the differences in the PAs (see above) and the yield of $[M - H]^-$ ions, therefore, depends strongly on the actual differences. For many matrices like 2, 5-DHB, the yields of deprotonated analytes such as peptides are typically substantially lower than those for their positively charged protonated counterparts and—for the above reasons—depend more strongly on the molecular composition of the analyte.

The PAs for some analyte molecules, for example oligosaccharides and synthetic polymers, are too low to favor proton transfer from the matrix. In positive-ion mode, these molecules are, therefore, preferentially detected as cationized species (*24*), mostly in the form of $[M + Na]^+$ or $[M + K]^+$ (because some alkali cations are ubiquitous; reaction 2.7). Given that the gas-phase acidities of these compounds can be comparatively high, deprotonated molecules of some of these compounds (e.g., many glycans) are more frequently detected. Sometimes these ions are observed in addition to alkali-adduct ions of the form $[M + (n + 1)\text{alkali} - n\text{H}]^+$, which may even dominate the mass spectrum. The use of matrices with particularly low cation affinities like dithranol may enhance the analyte cation yield (e.g., in the analysis of synthetic polymers). The latter class of compounds poses particularly high demands on the choice of matrix, solvent system, and preparation techniques (see Chapter 11 (this volume): *Synthetic Polymers*). Although listed under secondary ionization mechanisms, reaction (2.7a) proceeds in a direct reaction between analyte and metal cations available in the MALDI plume and thus does not require the matrix for the ionization, reaction (2.7b) indicates the second possible scenario (i.e., abtraction of a metal cation from a matrix-metal cation complex).

In exceptional cases, electron transfer from matrix to analyte (reaction 2.8) can yield analyte radical ions $M^{\bullet +}$.

Secondary reactions can also explain another classical feature of MALDI: the prevalence of singly charged ions (*24*). For small molecules, the Coulomb repulsion prohibits the transfer of a second proton or cation to an already charged molecule. Moreover, charge reduction of multiply charged ions, which can be formed by adduct ion formation with divalent metal ions like Cu^{2+} or Zn^{2+}, is energetically also favored (*24*).

Bibliography

(*1*) Karas, M.; Hillenkamp, F. Laser Desorption Ionization of Proteins with Molecular Masses Exceeding 10,000 daltons. *Anal. Chem.* **1988**, *60*, 2299–2301.

(*2*) Tanaka, K.; Waki, H.; Ido, Y.; Akito, S.; Yoshida, Y.; Yoshida, T. Protein and Polymer Analyses up to *m/z* 100,000 by Laser Ionization Time-of-flight Mass Spectrometry. *Rapid Commun. Mass Spectrom.* **1988**, *2*, 151–153.

(*3*) Cramer, R.; Richter, W. J.; Stimson, E.; Burlingame, A. L. Analysis of Phospho- and Glycopolypeptides with Infrared Matrix-Assisted Laser Desorption and Ionization. *Anal. Chem.* **1998**, *70*, 4939–4944.

(*4*) Dreisewerd, K.; Rohlfing, A.; Spottke, B.; Urbanke, C.; Henkel, W. Characterization of Whole Fibril-Forming Collagen Proteins of Types I, III, and V from Fetal Calf Skin by Infrared Matrix-Assisted Laser Desorption Ionization Mass Spectrometry. *Anal. Chem.* **2004**, *76*, 3482–3491.

(*5*) Horneffer, V.; Forsmann, A.; Strupat, K.; Hillenkamp, F.; Kubitscheck, U. Localization of Analyte Molecules in

MALDI Preparations by Confocal Laser Scanning Microscopy. *Anal. Chem.* **2001**, *73*, 1016–1022.
(*6*) Thomas, H.; Havlis, J.; Peychl, J.; Shevchenko, A. Dried-Droplet Probe Preparation on AnchorChip Targets for Navigating the Acquisition of Matrix-Assisted Laser Desorption/Ionization Time-of-Flight Spectra by Fluorescence of Matrix/Analyte Crystals. *Rapid Commun. Mass Spectrom.* **2004**, *18*, 923–930.
(*7*) Sze, E. T.; Chan, T. W.; Wang, G. Formulation of Matrix Solutions for Use in Matrix-Assisted Laser Desorption/Ionization of Biomolecules. *J. Am. Soc. Mass Spectrom.* **1998**, *9*, 166–174.
(*8*) Cramer, R.; Corless, S. Liquid Ultraviolet Matrix-Assisted Laser Desorption/Ionization Mass Spectrometry for Automated Proteomic Analysis. *Proteomics* **2005**, *5*, 360–370.
(*9*) Reiber, D. C.; Grover, T. A.; Brown, R. S. Identifying Proteins Using Matrix-Assisted Laser Desorption/Ionization In-Source Fragmentation Data Combined with Database Searching. *Anal. Chem.* **1998**, *70*, 673–683.
(*10*) Suckau, D.; Resemann, A. T3-Sequencing: Targeted Characterization of the N- and C-Termini of Undigested Proteins by Mass Spectrometry. *Anal. Chem.* **2003**, *75*, 5817–5824.
(*11*) Kocher, T.; Engstrom, A.; Zubarev, R. A. Fragmentation of Peptides in MALDI In-Source Decay Mediated by Hydrogen Radicals. *Anal. Chem.* **2005**, *77*, 172–177.
(*12*) Keough, T.; Youngquist, R. S.; Lacey, M. P. Sulfonic Acid Derivatives for Peptide Sequencing by MALDI MS. *Anal. Chem.* **2003**, *75*, 156A–165A.
(*13*) Cramer, R.; Corless, S. The Nature of Collision-Induced Dissociation Processes of Doubly Protonated Peptides: Comparative Study for the Future Use of Matrix-Assisted Laser Desorption/Ionization on a Hybrid Quadrupole Time-of-Flight Mass Spectrometer in Proteomics. *Rapid Commun. Mass Spectrom.* **2001**, *15*, 2058–2066.
(*14*) Suckau, D.; Resemann, A.; Schürenberg, M.; Hufnagel, P.; Franzen, J.; Holle, A. A Novel MALDI LIFT-TOF/TOF Mass Spectrometer for Proteomics. *Anal. Bioanal. Chem.* **2003**, *376*, 952–965.
(*15*) Laiko, V. V.; Baldwin, M. A.; Burlingame, A. L. Atmospheric Pressure Matrix-Assisted Laser Desorption/Ionization Mass Spectrometry. *Anal. Chem.* **2000**, *72*, 652–657.
(*16*) Loboda, A. V.; Krutchinsky, A. N.; Bromirski, M.; Ens, W.; Standing, K. G. A Tandem Quadrupole/Time-of-Flight Mass Spectrometer with a Matrix-Assisted Laser Desorption/Ionization Source: Design and Performance. *Rapid Commun. Mass Spectrom.* **2000**, *14*, 1047–1057.
(*17*) Shevchenko, A.; Loboda, A.; Ens, W.; Standing, K. G. MALDI Quadrupole Time-of-Flight Mass Spectrometry: A Powerful Tool for Proteomic Research. *Anal. Chem.* **2000**, *72*, 2132–2141.
(*18*) Ens, W.; Standing, K. G. Hybrid Quadrupole/Time-of-Flight Mass Spectrometers for Analysis of Biomolecules. In: *Biological Mass Spectrometry*; Burlingame, A. L., Ed.; Academic Press: New York, 2005; vol. 402, pp 49–78.
(*19*) Chernushevich, I. V.; Loboda, A. V.; Thomson, B. A. An Introduction to Quadrupole-Time-of-Flight Mass Spectrometry. *J. Mass Spectrom.* **2001**, *36*, 849–865.
(*20*) Laiko, V. V.; Moyer, S. C.; Cotter, R. J. Atmospheric Pressure MALDI/Ion Trap Mass Spectrometry. *Anal. Chem.* **2000**, *72*, 5239–5243.
(*21*) Qin, J.; Ruud, J.; Chait, B. T. A Practical Ion Trap Mass Spectrometer for the Analysis of Peptides by Matrix-Assisted Laser Desorption/Ionization. *Anal. Chem.* **1996**, *68*, 1784–1791.
(*22*) Chambers, D. M.; Goeringer, D. E.; McLuckey, S. A.; Glish, G. L. Matrix-Assisted Laser Desorption of Biological Molecules in the Quadrupole Ion Trap Mass Spectrometer. *Anal. Chem.* **1993**, *65*, 14–20.
(*23*) Dreisewerd, K. The Desorption Process in MALDI. *Chem. Rev.* **2003**, *103*, 395–426.
(*24*) Zenobi, R.; Knochenmuss, R. Ion Formation in MALDI Mass Spectrometry. *Mass Spectrom. Rev.* **2001**, *17*, 337–366.
(*25*) Vertes, A.; Gijbels, R.; Levine, R. D. Homogenous Bottleneck Model of the Matrix Assisted UV Laser Desorption of Large Molecules. *Rapid Commun. Mass Spectrom.* **1990**, *4*, 228.
(*26*) Lüdemann, H. C.; Redmond, R. W.; Hillenkamp, F. Singlet–Singlet Annihilation in Ultraviolet Matrix-Assisted Laser Desorption/Ionization Studied by Fluorescence Spectroscopy. *Rapid Commun. Mass Spectrom.* **2002**, *16*, 1287–1294.
(*27*) Dreisewerd, K.; Schürenberg, M.; Karas, M.; Hillenkamp, F. Influence of the Laser Intensity and Spot Size on the Desorption of Molecules and Ions in Matrix-Assisted Laser Desorption/Ionization with a Uniform Beam Profile. *Int. J. Mass Spectrom. Ion Processes* **1994**, *141*, 127.
(*28*) Schürenberg, M.; Dreisewerd, K.; Hillenkamp, F. Laser Desorption/Ionization Mass Spectrometry of Peptides and Proteins with Particle Suspension Matrixes. *Anal. Chem.* **1999**, *71*, 221–229.
(*29*) Zhiglei, L. V.; Garrison, B. J. Microscopic Mechanisms of Laser Ablation of Organic Solids in the Thermal and Stress Confinement Irradiation Regimes. *J. Appl. Phys.* **2000**, *88*, 1281–1298.
(*30*) Vogel, A.; Venugopalan, V. Mechanisms of Pulsed Laser Ablation of Biological Tissues. *Chem. Rev.* **2003**, *103*, 577–644.
(*31*) Berkenkamp, S.; Menzel, C.; Hillenkamp, F.; Dreisewerd, K. Measurements of Mean Initial Velocities of Analyte and Matrix Ions in Infrared Matrix-Assisted Laser Desorption Ionization Mass Spectrometry. *J. Am. Soc. Mass Spectrom.* **2002**, *13*, 209–220.
(*32*) Puretzky, A. A.; Geohegan, D. B. Gas-Phase Diagnostics and LIF-Imaging of 3-Hydroxypicolinic Acid MALDI-Matrix Plumes. *Chem. Phys. Lett.* **1998**, *286*, 425.
(*33*) Breuker, K.; Knochenmuss, R.; Zhang, J.; Stortelder, A.; Zenobi, R. Thermodynamic Control of Final Ion Distributions in MALDI: In-Plume Proton Transfer Reactions. *Int. J. Mass Spectrom.* **2003**, *226*, 211–222.
(*34*) Karas, M.; Glückmann, M.; Schäfer, J. Ionization in Matrix-Assisted Laser Desorption/Ionization: Singly Charged Molecular Ions are the Lucky Survivors. *J. Mass Spectrom.* **2000**, *35*, 1–12.
(*35*) Gimon-Kinsel, M.; Preston-Schaffter, L. M.; Kinsel, G. R.; Russel, D. H. Effects of Matrix Structure/Acidity on Ion Formation in Matrix-Assisted Laser Desorption Ionization Mass Spectrometry. *J. Am. Chem. Soc.* **1997**, *119*, 2534–2540.
(*36*) Mormann, M.; Bashir, S.; Derrick, P. J.; Kuck, D. Gas-Phase Basicities of the Isomeric Dihydroxybenzoic Acids and Gas-Phase Acidities of Their Radical Cations. *J. Am. Soc. Mass Spectrom.* **2000**, *11*, 544–552.

R. Cramer
University of Reading, Reading, UK

K. Dreisewerd
University of Münster, Münster, Germany